Magnetic Phases of Ultrathin Fe Grown on Cu(100) as Epitaxial Wedges

Dongqi Li, M. Freitag,* J. Pearson, Z. Q. Qiu,† and S. D. Bader
Materials Science Division, Argonne National Laboratory, Argonne, Illinois 60439
(Received 18 January 1994)

Magnetic wedges of Fe on Cu(100) are explored magneto-optically. In the region of 6–11 monolayers (ML) of fcc Fe grown at room temperature, in addition to a surface ferromagnetic layer with a Curie temperature ~250 K, the Fe bulk is antiferromagnetic with a Néel temperature of ~200 K. This fcc phase is stable only above a growth temperature of order ~200 K, below which the ferromagnetic spin-reorientation transition occurs at ~6 ML. The phase boundaries are delineated by cusps in the coercivity along the wedge.

PACS numbers: 75.70.Ak, 75.30.Kz, 75.30.Pd, 75.50.Bb

Iron is the most extensively studied magnetic element in the periodic table. It is located between antiferromagnetic Mn and ferromagnetic Co. The nearest-neighbor exchange interaction of Fe, as represented on a Bethe-Slater curve [1], can be positive (ferromagnetic) or negative (antiferromagnetic), and is structure sensitive. Thus, while bcc Fe is the prototypical ferromagnet, fcc Fe is predicted to support antiferromagnetic (AF), nonmagnetic, and ferromagnetic spin structures, depending upon the lattice constant [2]. Bulk fcc Fe (γ-Fe) exists only at elevated temperatures (>910 °C). However, γ-Fe can be stabilized as particles coherently precipitated from an fcc Cu host. The structure is then influenced by a periodic lattice distortion that supports an AF spin density wave, and the Néel transition at 67 K is first-order thermodynamically due to magnetoelastic couplings [3]. Epitaxial Fe films have been grown onto Cu(100) with contradictory results. For example, AF [4] and nonmagnetic [5,6] forms of Fe/Cu(100) have been identified, as well as surface [7] and bulk [4,5,8–11] ferromagnetic phases. Particularly striking is the recent report of a ferromagnetically live surface layer for 5–11 monolayers (ML) Fe grown at room temperature (RT) [7]. Also of interest is the identification of a spin-reorientation transition within a ferromagnetic film structure from perpendicular to in-plane easy axes of magnetization [9–11] for films grown at low temperature and subsequently annealed to RT. Additional work has correlated some of the magnetic phases with different structural reconstructions [7,12,13] and growth modes [14,15]. Extended x-ray-absorption fine structure (EXAFS) studies for RT-grown films [16] indicate a tetragonally distorted fcc phase (fct) initially, an fcc phase between 6 and 11 ML, and the bcc phase $\geq$ 11 ML. Theoretical calculations [17] indicate that the AF phase has a minimum in total energy that is nearly isotropic fcc, while the ferromagnetic phase has two minima associated with distorted fct structures.

In order to reconcile these results and provide a global picture of the Fe/Cu(100) system, we use wedge-shaped samples to investigate the magnetization detected magneto-optically as a function of both film thickness and substrate temperature during growth (T_s). We present a magnetic phase diagram for the growth of Fe/Cu(100) that has a variety of new features. First, we identify that the surface ferromagnetic phase, between 6 and 11 ML for RT-grown films, resides on top of AF Fe underlayers. Second, this AF phase possesses an enhanced Néel temperature T_N with respect to that of bulk γ Fe precipitates in Cu, though $T_N \lesssim T_C(s) \sim 250$ K, the surface Curie temperature. Third, this phase vanishes below T_s ~200 K, where the fct structure undergoes its ferromagnetic spin-reorientation transition. Finally, each of the three magnetic phase transitions studied herein (associated with the fct-to-fcc-to-bcc instabilities and with the fct spin reorientation) is found to be delineated by a cusp in the coercivity. The system Fe/Cu(100) shares a similar spin-reorientation transition with bcc Fe on Ag(100) due to competing magnetic anisotropies [18], but is more complex because of the interplay with multiple structural instabilities.

The Cu(100) substrate was initially prepared by mechanical polishing to 0.1 μm with alumina, followed by an electrochemical polishing [19]. A clean and well ordered Cu(100) surface was confirmed by reflecting high-energy electron diffraction (RHEED), low-energy electron diffraction (LEED), and Auger spectroscopy, after cycles of 1–2 keV Ar^+ sputtering and annealing at 600 °C in the ultrahigh vacuum chamber with base pressure of 1×10^{-10} Torr. Fe was evaporated from an alumina crucible. Typically the evaporation rate was ~0.7 Å/min, as monitored with a quartz-crystal oscillator and confirmed by RHEED oscillations within an accuracy of ~10%. The pressure during evaporation was $(2–5)\times10^{-10}$ Torr. Wedges were made by using a stepping motor to translate the substrate (nominally along the Cu ⟨011⟩ direction) behind a fixed mask during evaporation. A typical wedge had a slope of 1.5 ML/mm. More than twenty wedges were grown in the course of the study.

The magnetic properties of Fe/Cu(100) were monitored *in situ* by means of the surface magneto-optic Kerr-effect (SMOKE) [20]. A He-Ne laser beam was focused to ~0.2 mm diameter onto the film and was scanned along a wedge to get hysteresis loops from the Kerr signal for different Fe thicknesses. The normalized height of the loop

0031-9007/94/72(19)/3112(4)$06.00

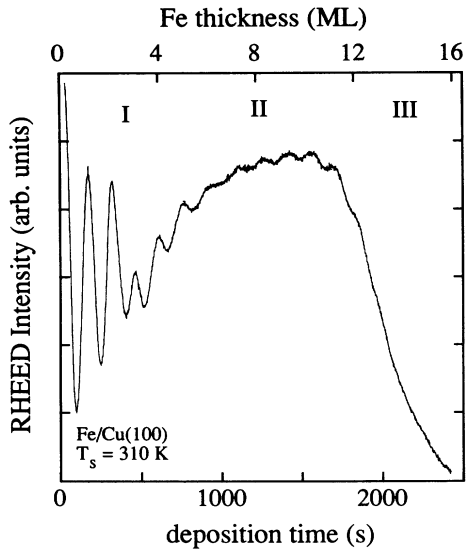

FIG. 1. RHEED intensity oscillations for Fe grown on Cu(100) at 310 K. Regions I, II, and III are labeled as in Ref. [9].

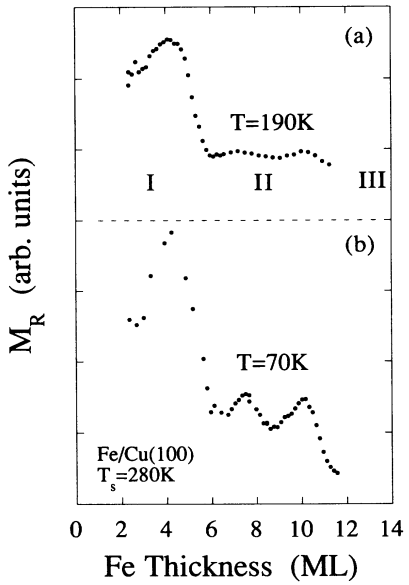

FIG. 2. M_R from polar SMOKE vs thickness across an Fe wedge grown at T_s=280 K and measured at 190 K (a) and 70 K (b). Regions I and III correspond to ferromagnetic fct and bcc phases, while region II has a live surface ferromagnetic layer and features that intensify upon cooling, attributed to AF Fe underlayers for which $T_N \leq T_C(s)$.

at zero field is proportional to the remanent magnetization (M_R), assuming that the magneto-optic response of the material is independent of thickness.

The growth mode was monitored by RHEED oscillations. Fe has been identified previously to grow onto Cu(100) in a nearly layer-by-layer mode for 5–11 ML of Fe when $T_s \sim$ RT [7,12]. Our RHEED oscillations, as shown in Fig. 1, are in agreement with those of Ref. [7]. In the notation of Ref. [7], we observe $n \times 1$ LEED patterns for 1–4 ML Fe films. The weak "3×1" patterns for thick films, as described in Ref. [12], serve as an indicator of the bcc Fe phase that appears after the RHEED oscillations stop. Although the 2×1 LEED beams are not observed for 6–11 ML fcc Fe, our samples are essentially the same in structure as the ones in previous work [7,16]. Films grown below RT were annealed to RT after deposition to improve the ordering while minimizing interfacial diffusion [15].

Figure 2(a) shows polar SMOKE results along an epitaxial Fe wedge. The sample was grown at T_s=280 K and is typical of samples grown at 270–310 K. There is an initial linear increase of the remanent Kerr signal between 1 and 4 ML of Fe, a relatively abrupt drop in signal at ~5–6 ML, followed by a thickness region between 6 and 11 ML for which the signal remains roughly constant at ~30%–40% of its maximum value, in agreement with Ref. [7]. (A change of magnetic easy axes from perpendicular to in plane occurs at 11–12 ML, but is not shown in Fig. 2.) Based on EXAFS studies [16], the initial ferromagnetic region corresponds to the fct phase, while the region with surface ferromagnetism between 6 and 11 ML corresponds to fcc Fe.

In addition to reproducing the results of Ref. [7] we have additional new observations that are not provided by previous investigations. In the region where Ref. [7] finds that the signal is independent of thickness (6–11 ML), we observe that upon cooling a two-peaked M_R behavior develops, as shown in Fig. 2(b). At 70 K, the peak separation is ~2.6 ML, and the amplitude of the intensity difference between the first peak and the valley (ΔM_R) is ~24% of the average Kerr signal between 6 and 11 ML. Since SMOKE measures the total magnetic signal of all the layers at this thickness range, such a variation with thickness suggests that the perpendicular component of the net magnetic moment oscillates with thickness. There is no longitudinal Kerr signal detected in this same thickness region, setting the upper limit of the net in-plane component of magnetic moment to ~5%. This rules out the possibility of a canted spin structure, where the net moment remains fixed and only changes its orientation with respect to the surface normal.

We attribute our results to a ferromagnetic surface with AF Fe underlayers with alternating sheets of spins for which $T_N \lesssim T_C$(s). With the total number of these spin sheets changing between even and odd, the net moment, and therefore the Kerr rotation, would oscillate with thickness. In Fig. 3 the Kerr signal at the valley and ΔM_R are shown for different samples as a function of temperature. A linear extrapolation of ΔM_R defines an intercept at $\sim$ 200 K, while M_R vanishes at ~250 K. Thus, we estimate $T_C(s) = 250 \pm 20$ K, as in Ref. [7], while T_N ~200 K. Note that this value of T_N is significantly higher than that for the low-moment γ-Fe particles in a Cu host (~67 K [21]). Also, if we suppose that the

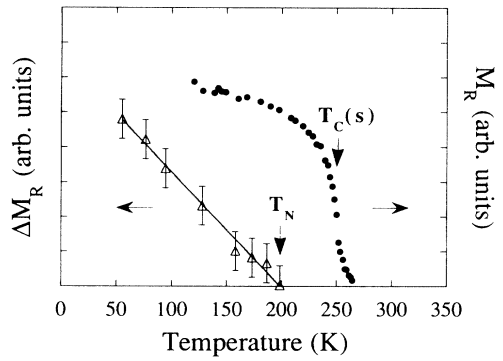

FIG. 3. Temperature dependence of M_R and of the peak-to-valley difference ΔM_R for two wedges grown at $T_s = 300$ K, showing $T_C(s)$ and T_N, respectively.

magneto-optic response of the fcc phase (6–11 ML Fe) is the same as that for the fct phase (1–5 ML Fe), then the fcc surface magnetization is at least 1.6 times that for one fct Fe monolayer. Thus, it is plausible that the top *two* layers of the fcc Fe are ferromagnetic. The enhanced value of T_N, the even larger value of $T_C(s)$, and the sizable magneto-optic signals for fcc Fe (6–11 ML Fe) suggest that the magnetic moment for this phase may be considerably larger than the $0.7\mu_B$ of γ-Fe precipitates [21]. The peak separation in Fig. 2 of $\sim$ 2.6 ML, rather than 2 ML, suggests a possible role for spin density wave (SDW) structures, as occurs for the bulk γ-Fe precipitates, which may relate to the quantum-well states that occur in ultrathin films with nonintegral periods [19] as governed by Fermi surface effects [19,22].

Another new observation is that the structural and magnetic phase transformations along the wedges are delineated by cusps in the coercivity H_c, as shown in Fig. 4. The cusp in H_c at the structural phase transitions must be related to the mixed phases and the relevant domain structures.

Figure 5 illustrates representative SMOKE results for wedges grown at different temperatures. The thickness range of stability of the fcc phase (ferromagnetic surface and AF underlayers) becomes smaller for films grown at lower values of T_s and eventually disappears below $T_s \sim 200$ K. Below this value of T_s the magnetic spin-reorientation transition ensues in the fct phase. This raises the interesting question of whether or not this spin reorientation is accompanied by an fct-to-bcc structural transition. The LEED patterns, though diffuse, still indicate the fourfold pseudomorphy of fct-Fe at 7–8 ML and lack the "3×1" bcc signature [12]. The spin-reorientation transition at 5–6 ML Fe for $T_s \leq 200$ K is therefore fundamentally distinct from that at 11–12 ML Fe for RT growth, where the bcc transition occurs. This conclusion supports the previous thought that it is the magnetic anisotropy changes with thickness that drive the spin-reorientation transition at 5–6 ML.

Figure 6 summarizes our results with a map of the

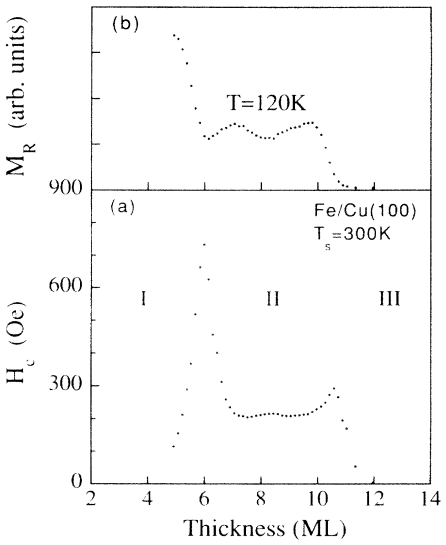

FIG. 4. (a) H_C along a wedge. Cusps at $\sim$ 6.0 and 10.6 ML coincide with the transitions in (b) from region I to II and II to III.

proposed boundaries for both the transition from ferromagnetic to AF bulk, and for the spin reorientation from perpendicular to in plane, as well as for bcc conversion. The location of the boundary between the AF (fcc) phase II(a) and the ferromagnetic (fct) phase II(b), though difficult to place accurately, occurs roughly in the vicinity where $T_s \sim T_N \sim T_C(s)$, suggestive that magnetostriction energetics may favor the fct phase over fcc.

The formation of different Fe phases vs thickness and T_s can be understood qualitatively. Structurally there is the competition between bulk bcc Fe and the epitaxial face-centered phases. The lattice mismatch (3.61 Å

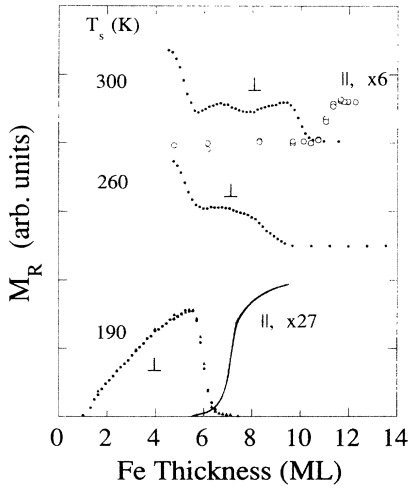

FIG. 5. Magneto-optical signals for Fe wedges grown at different T_s values. Solid symbols are polar signals and open circles and curves indicate longitudinal signals. (Measurements at 120, 140, and 110 K, respectively, from top to bottom.)

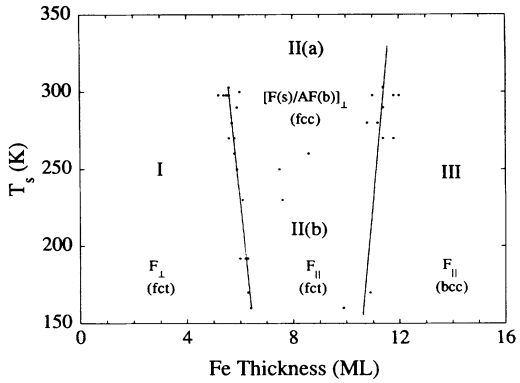

FIG. 6. Magnetic phase diagram with respect to growth temperature and thickness. In region I, films are ferromagnetic with perpendicular easy axes (fct). In region II(a) the surface is ferromagnetic while the underlayers are AF (fcc). In region II(b), films are ferromagnetic with in-plane easy axes (fct). In region III, the films are ferromagnetic with in-plane easy axes (bcc). (Measurements at 110–190 K.)

for Cu and 3.59 Å for fcc Fe) tends to favor the fct over fcc. The tetragonal distortion stabilizes ferromagnetic Fe with perpendicular magnetization axes. Epitaxial strain relaxes with increasing thickness and growth temperature. Thus, as the fct phase thickens at $T_s \sim$ RT, the structure relaxes into the fcc phase, which prefers AF ordering, as in the γ-Fe bulk precipitates. However, surface relaxation in the fcc films presumably enhances the surface magnetic moment and stabilizes the ferromagnetic live layer. Correspondingly, as the fct phase thickens for low T_s it retains its stability because interfacial strain persists, due to magnetostriction effects [23] and the lack of a sufficiently intermixed buffer layer. This permits the magnetic energetics to govern the spin-reorientation transition in which the shape anisotropy overcomes the surface anisotropy.

Seemingly contradictory results can now be understood. For example, Thomassen *et al.* [7] limited their study to RT growth, and thus bypassed the spin-reorientation studied by Pappas *et al.* [10] and Liu *et al.* [9] for low-T_s grown films. The ongoing controversy as to whether fcc Fe is ferromagnetic or AF becomes moot, in that most previous work can be accommodated within the new phase diagram. The message is that nanoscale fcc Fe is subject to strain and lattice distortions that can stabilize diverse magnetic states.

This work was supported by the U.S. DOE BES-Materials Sciences under Contract No. W-31-109-ENG-38.

* Visitor from Forschungszentrum Jülich, IGV, Postfach 1913, 52425 Jülich, Germany.

† Permanent address: Department of Physics, University of California, Berkeley, CA 94720.

[1] J. S. Kouvel and R. H. Wilson, J. Appl. Phys. **32**, 435 (1961).

[2] C. S. Wang, B. M. Klein, and H. Krakauer, Phys. Rev. Lett. **54**, 1852 (1985); V. L. Moruzzi *et al.*, Phys. Rev. B **34**, 1784 (1986); F. J. Pinski *et al.*, Phys. Rev. Lett. **56**, 2096 (1986).

[3] Y. Tsunoda, N. Kunitomi, and R. M. Nicklow, J. Phys. F **17**, 2447 (1987).

[4] W. A. A. Macedo and W. Keune, Phys. Rev. Lett. **61**, 475 (1988); W. A. A. Macedo, W. Keune, and E. D. Ellerbrock, J. Magn. Magn. Mater. **93**, 552 (1991).

[5] P. A. Montano *et al.*, Phys. Rev. Lett. **59**, 1041 (1987); S. D. Bader and E. R. Moog, J. Appl. Phys. **61**, 3729 (1987).

[6] A. A. Hezaveh *et al.*, Solid State Commun. **57**, 329 (1986).

[7] J. Thomassen *et al.*, Phys. Rev. Lett. **69**, 3831 (1992).

[8] M. F. Onellion *et al.*, Phys. Rev. B **33**, 7322 (1986); D. Pescia *et al.*, Phys. Rev. Lett. **58**, 2126 (1987); F. J. Himpsel, Phys. Rev. Lett. **67**, 2363 (1991).

[9] C. Liu, E. R. Moog, and S. D. Bader, Phys. Rev. Lett. **60**, 2422 (1988).

[10] D. P. Pappas, K.-P. Kämper, and H. Hopster, Phys. Rev. Lett. **64**, 3179 (1990); D. P. Pappas, C. R. Brundle, and H. Hopster, Phys. Rev. B **45**, 8169 (1992).

[11] R. Allenspach and A. Bischof, Phys. Rev. Lett. **69**, 3385 (1992).

[12] P. Xhonneux and E. Courtens, Phys. Rev. B **46**, 556 (1992); F. Scheurer *et al.*, Phys. Rev. B **48**, 9890 (1993).

[13] P. Bayer *et al.*, Phys. Rev. B **48**, 17611 (1993).

[14] D. D. Chambliss *et al.*, in *Magnetic Ultrathin Films*, edited by B. T. Jonker *et al.*, MRS Proceeding Vol. 313 (Materials Research Society, Pittsburgh, 1993), p. 713, and references therein; K. E. Johnson *et al.*, J. Vac. Sci. Technol. A **11**, 1654 (1993); M. Wuttig and J. Thomassen, Surf. Sci. **282**, 237 (1993); A. Brodde and H. Neddermeyer, Surf. Sci. **287/288**, 988 (1993).

[15] W. F. Egelhoff, Jr. and I. Jacob, Phys. Rev. Lett. **62**, 921 (1989); D. A. Steigerwald, I. Jacob, and W. F. Egelhoff, Jr., Surf. Sci. **202**, 472 (1988).

[16] H. Magnan *et al.*, Phys. Rev. Lett. **67**, 859 (1991).

[17] S. S. Peng and H. J. F. Jansen, J. Appl. Phys. **69**, 6132 (1991).

[18] Z. Q. Qiu, J. Pearson, and S. D. Bader, Phys. Rev. Lett. **70**, 1006 (1993).

[19] J. E. Ortega *et al.*, Phys. Rev. B **47**, 1540 (1993); F. J. Himpsel and J. E. Ortega, Phys. Rev. B **46**, 9719 (1992).

[20] S. D. Bader, J. Magn. Magn. Mater. **100**, 440 (1991).

[21] G. J. Johanson, M. B. McGirr, and D. A. Wheeler, Phys. Rev. B **1**, 3208 (1970); S. C. Abrahams, L. Guttman, and J. S. Kasper, Phys. Rev. **127**, 2052 (1962).

[22] M. D. Stiles, Phys. Rev. B **48**, 7238 (1993).

[23] See discussion in G.G. Hembree *et al.*, "Field Induced Metastable States in Ultrathin Films of fcc Fe/Cu(100)," Appl. Phys. Lett. (to be published).